E-cadherin represses anoikis resistance in sarcomas through both signaling and mechanical mechanisms

Mohit Kumar Jolly[1#], Kathryn E. Ware[2#], Shengnan Xu[2], Shivee Gilja[2], Samantha Shetler[2], Yanjun Yang[1, 3], Xueyang Wang[4], R. Garland Austin[2], Alexander J. Hish[2], Suzanne Bartholf DeWitt[5], Jason T George[1,6,7], R. Timothy Kreulen[8], Mary-Keara Boss[9], Alexander L. Lazarides[8], David L. Kerr[8], Drew G. Gerber[2], Andrew J. Armstrong[10,11], Mark W. Dewhirst[12], William C. Eward[8], Herbert Levine[1,6], and Jason A. Somarelli[2]

[1]Center for Theoretical Biological Physics, Rice University, Houston, Texas, USA; [2]Department of Medicine, Duke University Medical Center, Durham, North Carolina, USA; [3]Department of Applied Physics, Rice University, Houston, Texas, USA; [4]School of Medicine, Johns Hopkins University, Baltimore, Maryland, USA; [5]Department of Pathology, Duke University Medical Center, Durham, North Carolina, USA; [6] Department of Bioengineering, Rice University, Houston, Texas, USA; [7]Medical Scientist Training Program, Baylor College of Medicine, Houston, TX, USA; [8]Department of Orthopaedics, Duke University Medical Center, Durham, North Carolina, USA; [9]Flint Animal Cancer Center, Colorado State University, Fort Collins, Colorado, USA; [10]Solid Tumor Program and [11]Duke Prostate Center, Duke University Medical Center, Durham, North Carolina, USA; [12]Department of Radiation Oncology, Duke University Medical Center, Durham, North Carolina, USA

#These authors contributed equally to this work.

*Address correspondence to jason.somarelli@duke.edu

Key words: anchorage-independent growth, phenotypic plasticity, E-cadherin, TBX2, CREB

Abstract

E-cadherin, an epithelial-specific cell-cell adhesion molecule, plays multiple roles in maintaining adherens junctions, regulating migration and invasion, and mediating intracellular signaling. Downregulation of E-cadherin is a hallmark of epithelial-mesenchymal transition (EMT) and correlates with poor prognosis in multiple carcinomas. Conversely, upregulation of E-cadherin is prognostic for improved survival in sarcomas. Yet, despite the prognostic benefit of E-cadherin expression in sarcoma, the mechanistic significance of E-cadherin in sarcomas remains poorly understood. Here, by combining mathematical models with wet-bench experiments, we identify the core regulatory networks mediated by E-cadherin in sarcomas, and decipher their functional consequences. Unlike in carcinomas, E-cadherin overexpression in sarcomas does not induce a mesenchymal-epithelial transition (MET). However, E-cadherin acts to reduce both anchorage-independent growth and spheroid formation of sarcoma cells. Ectopic E-cadherin expression acts to downregulate phosphorylated CREB (p-CREB) and the transcription factor, TBX2, to inhibit anoikis resistance. RNAi-mediated knockdown of TBX2 phenocopies the effect of E-cadherin on p-CREB levels and restores anoikis sensitivity to sarcoma cells. Beyond its signaling role, E-cadherin expression in sarcoma cells can also strengthen cell-cell adhesion and restricts spheroid growth through mechanical action. Together, our results demonstrate that E-cadherin inhibits sarcoma aggressiveness by inducing anoikis and restricting colony growth.

Introduction

Sarcomas – deadly cancers that arise from tissues of a mesenchymal lineage – are highly aggressive, with five year survival rates of just 66% (Siegel et al., 2017). Despite their mesenchymal origin, some sarcomas undergo phenotypic plasticity in which they gain "epithelial-like" traits (Somarelli et al., 2016; Tian et al., 2013; Yin et al., 2012). One might expect the acquisition of epithelial-like traits to be of little relevance in mesenchymal tumors, yet that is not the case. Phenotypic plasticity is clinically important in sarcoma patients: Sarcoma patients whose tumors express epithelial-like biomarkers have improved outcomes relative to patients with more "mesenchymal-like" tumors (Somarelli et al., 2016; Tian et al., 2013; Wang et al., 2015a; Yin et al., 2012).

Phenotypic plasticity observed in sarcomas is reminiscent of the phenomenon of epithelial plasticity in carcinomas. Epithelial plasticity refers to reversible transitions between epithelial and mesenchymal phenotypes. In carcinomas, the phenotypic transition to a more mesenchymal-like state via an epithelial-mesenchymal transition (EMT) promotes migratory and invasive gene expression programs that facilitate cancer cell invasion and metastatic seeding (Nieto et al., 2016). Subsequent to metastatic dissemination, a reversion to an epithelial-like state via mesenchymal -epithelial transition (MET) re-awakens proliferative signals within the metastatic niche to enable metastatic colonization (Nieto et al., 2016).

In carcinomas, the gene expression programs that control EMT/MET are regulated at multiple stages, including through epigenetics (Tam and Weinberg, 2013), transcription (De Craene and Berx, 2013), microRNAs (Lu et al., 2013), alternative splicing (Brown et al., 2011; Jia et al., 2017), and post-translational protein stability (De Herreros et al., 2010). These regulatory mechanisms control genes involved in cell polarity, cytoskeletal architecture, cell-substrate adhesion, and cell-cell adhesion. One of these genes, E-cadherin, is an epithelial-specific cell-cell adhesion molecule that has multiple functions in maintenance of adherens junctions (Lewis et al., 1995), cytoskeletal organization (Chen et al., 2014), migration (Chen and Obrink, 1991; Jolly et al., 2017a), and intracellular signaling (Orsulic et al., 1999). Downregulation of E-cadherin is a marker of poor prognosis in multiple cancers of an epithelial origin (Hong et al., 2011; Li et al., 2017). In addition, loss-of-function germline mutations in E-cadherin predispose individuals to familial gastric cancer (Guilford et al., 1998), early onset colorectal cancer (Richards et al., 1999), and hereditary lobular breast cancer (Corso et al., 2016).

Consistent with its known tumor suppressor role in carcinomas, E-cadherin upregulation is also prognostic for improved survival in sarcomas (Wang et al., 2015b). However, despite the prognostic importance of E-cadherin in sarcomas, little is known about the molecular mechanisms that underlie improved outcomes of E-cadherin upregulation in mesenchymally-derived cancers. Here, we use a combined theoretical-experimental approach to decipher the gene regulatory networks driven by E-cadherin in sarcomas. Unlike in many carcinomas, in which E-cadherin is sufficient to induce a more epithelial-like phenotype (Chao et al., 2010), ectopic over-expression of E-cadherin in sarcomas did not alter epithelial plasticity biomarkers,

104 migration, or invasion. E-cadherin expression did, however, significantly inhibit both anoikis
105 resistance and spheroid growth in sarcoma cells. Non-cancer cells that become detached from the
106 normal tissue architecture undergo a cell death program known as anoikis. Resistance to anoikis
107 is a hallmark of cancer progression and of an aggressive phenotype. E-cadherin-mediated
108 repression of anoikis resistance was accompanied by downregulation of phospho-CREB and the
109 transcription factor, TBX2. TBX2 knockdown led to reductions in total and phospho-CREB and
110 phenocopied E-cadherin-mediated inhibition of anoikis resistance. In addition to its signaling
111 role, E-cadherin repressed spheroid size through increased cell-cell adhesion. Together, these
112 results indicate that E-cadherin acts through both signaling and mechanical roles to inhibit
113 sarcoma aggressiveness by suppressing anoikis resistance and spheroid growth.
114
115 **Materials and Methods**
116 Analysis of the prognostic impact of E-cadherin in clinical data sets
117 The prognostic significance of E-cadherin in osteosarcoma was analyzed using the R2:
118 Genomics Analysis and Visualization Platform (https://hgserver1.amc.nl/cgi-bin/r2/main.cgi).
119 Kaplan Meier plots of metastasis-free survival and overall survival were constructed using the
120 Kaplan Meier option with the 'mixed osteosarcoma' dataset (Kuijjer, Rydbeck et al. 2012). For
121 soft tissue sarcomas, Kaplan Meier plots were constructed in JMP13.0 as previously described
122 (Somarelli, Shetler et al. 2016) using E-cadherin RNA-Seq and protein levels from The Cancer
123 Genome Atlas (TCGA). Correlations between E-cadherin levels and EMT score were performed
124 using RNA-Seq data from TCGA and analyzed in JMP13.0.
125
126 To calculate EMT scores, raw TCGA sarcoma gene expression data for 259 samples was
127 accessed from the R2: Genomics Analysis and Visualization Platform (http://r2.amc.nl). EMT
128 quantification was applied by using a small set of EMT-predictors in addition to a normalization
129 signature of EMT-uncorrelated transcripts as described previously (George, Jolly et al. 2017).
130 Each sample was assigned an EMT score, $0 < \mu < 2$, with E scores $\mu_E < 0.5$, M scores $\mu_M > 1.5$
131 and hybrid E/M scores $0.5 \leq \mu_{E/M} \leq 1.5$ intermediary to both E and M scores. Samples were
132 partitioned into E-cadherin^{low} and E-cadherin^{high} categories based on median E-cadherin
133 expression. The probability distribution for each group was estimated by spline interpolation of
134 the empirical EMT score histogram.
135
136 Cell culture conditions, ectopic E-cadherin expression, and flow cytometry
137 143B, U2OS, Abrams, and RD cells were cultured in high glucose Dulbecco's Modified Eagle's
138 Medium (DMEM) supplemented with 10% fetal bovine serum (FBS) and 1%
139 penicillin/streptomycin (pen-strep) at 37°C and 5% CO_2 in a humidified incubator. 143B, U2OS,
140 and RD cells were obtained from the Duke University Cell Culture Facility, which performs
141 routine mycoplasma testing and verifies cell identity by analysis of short tandem repeats. Abrams
142 cells were a gift of Dr. Douglas Thamm (Colorado State University). To generate sarcoma cells
143 stably expressing E-cadherin, 143B, U2OS, and RD cells were stably transfected with an empty

144 vector (pcDNA3) or hE-cadherin-pcDNA3 (a gift from Barry Gumbiner; Addgene plasmid #
145 45769; (Gottardi, Wong et al. 2001)). E-cadherin positive cells were sorted by flow cytometry
146 using a PerCP710 anti-E-cadherin antibody (eBioscience cat. 46-3249). To do this, confluent
147 cells in a T75 flask were washed with phosphate buffered saline (PBS), scraped, pelleted by
148 centrifugation at 250 x g for 10 minutes, resuspended in 5% bovine serum albumin in PBS,
149 incubated for 30 minutes, centrifuged as above, resuspended in anti-E-cadherin antibody dilution
150 at 5 µL in 100 µL of DMEM with 5% FBS per 1 x 10^6 cells, incubated for 30 minutes,
151 centrifuged again, washed with 5 ml of PBS, spun, resuspended in 0.5 ml of DMEM
152 supplemented with 5% FBS, and filtered through a 30 µM filter (Partek) into a flow cytometry
153 tube. E-cadherin+ cells were sorted into fully supplemented DMEM at the Duke University Flow
154 Cytometry Shared Resource.

155 Knockdown by siRNAs

156 A total of 20 nM of Allstars non-silencing (Qiagen) or target gene siRNA (Qiagen) was diluted
157 in Opti-MEM and mixed with Lipofectamine RNAiMax diluted in Opti-MEM. The RNAiMax-
158 siRNA mixtures were incubated for 20 minutes at room temperature, followed by plating of the
159 mixtures in 24-well plates. A total of 25,000 cells/well diluted in fully supplemented DMEM
160 were seeded atop the RNAiMax-siRNA mixtures and incubated overnight at 37°C and 5% CO_2
161 in a humidified incubator. Media was replaced the next day. After 72 hours of incubation, cells
162 were collected in the appropriate buffer or fixative for downstream applications.
163

164 Gene expression analysis by qRT-PCR

165 RNA was extracted from cultured cells using the Zymo Quick RNA Miniprep Kit following the
166 manufacturer's protocol. Reverse transcription (RT) reactions were performed as described
167 (Somarelli et al. 2016) using the ABI High Capacity cDNA Reverse Transcription Kit
168 (ThermoFisher). RT reactions were incubated following the manufacturer's protocol in a
169 SimpliAmp thermocycler (Life Technologies). RT reactions were diluted 1:5 in nuclease-free
170 H2O, and RT-qPCR was performed as described (Somarelli et al. 2016) in a Vii7 real time-PCR
171 detection system (Applied Biosystems).
172

173 Western blotting, immunofluorescence staining, phospho-kinase arrays, and ELISAs

174 Western blotting and immunofluorescence staining were performed as previously described
175 (Somarelli et al. 2016). A complete list of primary antibodies and their dilutions is provided in
176 the Supplementary Text. To prepare lysates for phospho-kinase arrays, E-cadherin$^-$ and E-
177 cadherin$^+$ cells were sorted by flow cytometry prior to each assay, seeded into 10 cm dishes, and
178 allowed to grow for 48-72 hours until they reached 80% confluence. Cells were then washed
179 twice with ice-cold PBS and scraped gently in 2 ml of PBS using cell scrapers. Cells were
180 counted using the CountessII system (Life Technologies), and cells were solubilized at 1 x 10^7
181 cells/ml in Lysis Buffer 6 provided as part of the Proteome Profiler Human Phospho-Kinase
182 Array Kit (R&D Systems). Total protein concentrations in 143B+empty vector and 143B+E-
183 cadherin lysates were estimated using a combination of both Bradford assays and western

184 blotting (to analyze consistent loading of intact protein with β-actin as a loading control). Lysates
185 were used in the Proteome Profiler Human Phospho-Kinase Array (R&D cat. ARY003b)
186 according to the manufacturer's instructions. Membranes were exposed to x-ray films and
187 visualized on a light box. The same procedure was used to generate lysates for ELISAs, and p-
188 CREB levels were quantified using DuoSet IC Human/Mouse/Rat Phospho-CREB (S133)
189 ELISA kits (R&D Systems).
190
191 Migration, invasion, proliferation, soft agar, spheroid growth assays and cell-cell adhesion assays
192 For migration and invasion assays, a total of 500 µL of DMEM (with 10% FBS and 1%
193 pen/strep) was added to the top and bottom of Boyden chamber wells for two hours to hydrate
194 the transwell membranes. Next, 50,000 cells per well diluted in 500 µL of serum-free DMEM
195 was added to the top of the chambers, with 500 µL of media containing 10% FBS in the bottom
196 chambers. Cells were incubated for 24 hours, after which the tops of the chambers were scrubbed
197 with sterile cotton swabs, and the bottoms were fixed in 4% paraformaldehyde (PFA) for 15
198 minutes, permeabilized in 0.2% Triton X-100 in PBS for 30 minutes, blocked in 5% BSA in PBS
199 for 30 minutes, and stained with Hoechst dye (1:2,000 dilution) for one hour. Images were
200 captured at 40X total magnification via epifluorescence microscopy, and cells were counted
201 using ImageJ. Invasion was calculated as the proportion of cells migrating through Matrigel-
202 coated chambers divided by the number of cells migrating through uncoated chambers.
203 Scratch wound migration assays were performed in 96-well plates for 143B cells and in
204 24-well plates for RD cells. 143B cells were seeded at 20,000 cells per well and incubated
205 overnight, after which scratches were made in the wells using a WoundMaker (Essen
206 Biosciences). For RD cells, 200,000 cells per well were seeded and incubated overnight.
207 Scratches were made using a 20-200 µl pipette tip. For both cell types, wells were washed with
208 PBS, and replaced with fully supplemented DMEM. Images were captured every two hours
209 using the IncuCyte Zoom Live Cell Imaging System. Scratch wound migration of 143B cells was
210 analyzed using the migration analysis module in the IncuCyte Zoom software, and migration of
211 RD cells was analyzed using ImageJ.
212 For monolayer proliferation assays, 25,000 cells per well were plated in 500 µL of
213 DMEM in 24-well plates, and percent confluence was analyzed using the IncuCyte Zoom
214 software, with imaging at two hour intervals at 100X total magnification.
215 Soft agar anchorage-independent growth assays were performed as previously described
216 (Borowicz, Van Scoyk et al. 2014). Briefly, 25,000 cells were embedded in a 0.3% agarose layer
217 atop a bottom layer of 0.5% agarose and cultured for approximately three weeks in fully
218 supplemented DMEM in 6-well plates. Media was replenished weekly, after which colonies were
219 stained with Nitrotetrazoleum Blue overnight, plates were imaged, and colonies counted using
220 ImageJ.
221 For spheroid growth assays, cells were scraped in fully supplemented DMEM, and 1,000
222 cells/well were seeded in ultra-low attachment plates (Costar, cat. #7007).

For cell-cell adhesion assays, 12-well plates were incubated overnight with 0.5%BSA/Fraction V in CMFS buffer at 4°C. CMFS buffer contains 4 g NaCl, 0.2g KCl, 0.03g Na_2HPO_4, and 0.5 g glucose diluted in 500 ml PBS (-/-). Plates were washed with CMFS buffer and 200,000 cells were immediately seeded in 1mL of media. Plates were incubated on an orbital shaker at 100 rpm at 37°C for 3 hours, followed by the addition of 1.5 mL of 4% PFA and incubated at room temperature for 30 minutes. Cells aggregates were immediately quantified in size categories using ImageJ.

Statistical analyses

All data were analyzed for statistically significant differences using the Student's t-test (for two comparisons) or analysis of variance with Tukey's post-hoc correction (for multiple comparisons) in JMP Pro 13. Any p-value < 0.05 was considered statistically significant.

Quantitative modeling for simulating the mechanical effects of E-cadherin

We use a two-dimensional subcellular elements model (Basan et al., 2013; Zimmermann et al., 2016; (Yang and Levine 2018)) to simulate the effects of different levels of E-cadherin, where each cell is represented by two subcellular elements, the front and rear element (inserted cartoon in Fig. 7B (Zimmermann et al., 2016)). Each subcellular element is self-propelled with a self-propulsion force m, which balances the intracellular contraction f_{contr} between the front and rear element. We use a long range attractive and short range repulsive intercellular force $f_{rep/adh}$ to model cell-cell adhesion (E-cadherin level) and volume exclusion, respectively. There is a friction between each subcellular element and the substrate with a constant coefficient ξ. The velocity and position for each subcellular element is updated by: $v = 1/\xi\ (m + f_{contr} + f_{rep/adh})$, and $x = vdt$. In our simulation, cells can divide with a probability based on its size (Zimmermann et al., 2016). Once the cell length exceeds a certain threshold, it divides at a given probability. Upon division, two new subcellular elements are inserted, forming two new cells. This process simulates the cell cycle: the expansion of cell culture is driven by contact inhibition of locomotion, and cells are elongated during the expansion.

Quantitative mathematical modeling of E-cadherin regulatory network in anoikis resistance

A mathematical model representing the interactions among E-cadherin, TBX2, NRAGE, and their effects on anoikis sensitivity was constructed. The set of coupled ordinary differential equations (ODEs) representing the dynamics of these molecular species was simulated in MATLAB (Mathworks Inc.). The details of model construction and parameters used is given in supplemental methods.

Results

Aberrant E-cadherin expression in sarcomas is prognostic for improved clinical outcomes

261 Our previous work found that phenotypic plasticity in sarcomas leads to a more epithelial-like
262 phenotype (Somarelli et al., 2016). This transition to a more epithelial gene expression program
263 has prognostic relevance: Compared to patients whose sarcomas are more strongly
264 mesenchymal-like, patients with epithelial-like sarcomas have improved overall survival
265 (Somarelli et al., 2016). One of the hallmarks of this mesenchymal-epithelial transition (MET) is
266 upregulation of the epithelial cell-cell adhesion molecule, E-cadherin. To further understand the
267 prognostic relevance of E-cadherin in sarcomas, we stratified osteosarcoma patients into E-
268 cadherin^{high} and E-cadherin^{low} groups using publicly-available RNA-Seq data (Kuijjer et al.,
269 2012). E-cadherin^{high} patients had improved metastasis-free survival (**Figure 1A**) and overall
270 survival compared to E-cadherin^{low} patients (**Figure 1B**). Likewise, soft tissue sarcoma (STS)
271 patients from The Cancer Genome Atlas with higher E-cadherin mRNA trended toward better
272 overall survival than patients with lower E-cadherin (**Figure 1C**) while patients with higher E-
273 cadherin protein had significantly improved overall survival compared to patients with lower E-
274 cadherin protein levels (**Figure 1D**). These analyses suggest that E-cadherin has prognostic
275 utility in sarcomas.
276
277 <u>Ectopic E-cadherin expression in sarcomas does not promote MET</u>
278 While it is clear that E-cadherin has prognostic relevance in sarcomas, the underlying molecular
279 mechanism(s) and cellular phenotypes by which E-cadherin contributes to a less aggressive
280 tumor remain unknown. Given the important role of E-cadherin as a mediator of the epithelial
281 phenotype, we hypothesized that E-cadherin may promote an MET-like phenotype in sarcomas,
282 including suppression of migration and invasion pathways. Consistent with this hypothesis, E-
283 cadherin expression in sarcomas is inversely correlated with an EMT signature; sarcomas with a
284 more mesenchymal-like gene expression program have lower E-cadherin while those with a
285 more epithelial-like gene expression program have higher E-cadherin (**Figure 2A**). To test the
286 hypothesis that E-cadherin inhibits sarcoma aggression by promoting an MET-like phenotypic
287 switch, we ectopically expressed E-cadherin in RD human rhabdomyosarcoma and 143B human
288 osteosarcoma cells and assayed for changes in cell growth. We found E-cadherin expression had
289 no effect on the growth of cells in monolayer (**Supplementary Figure 1A-F**). We next assayed
290 for changes in EMT biomarkers by qRT-PCR. With the exception of a statistically significant
291 two-fold reduction in Slug in 143B cells, E-cadherin had no significant effect on EMT markers
292 (**Figure 2B, Supplementary Figure 2A**). Consistent with these results, E-cadherin expression
293 did not alter scratch wound migration (**Figure 2C**) or invasion in 143B cells (**Figure 2D**) or in
294 RD cells **(Supplementary Figure 2B-C)**. We next asked if E-cadherin status changed the overall
295 EMT score using our previously-derived scoring metric for epithelial, mesenchymal and hybrid
296 epithelial/mesenchymal states (George et al., 2017). Using our scoring metric, we calculated
297 EMT scores for E-cadherin^{high} vs. E-cadherin^{low} expressing osteosarcomas. The scoring metric
298 was strongly mesenchymal for all sarcomas analyzed, regardless of E-cadherin status, suggesting
299 that E-cadherin was not capable of lineage reprogramming toward an epithelial-like state in
300 sarcomas (**Figure 2E**). Visualization of the EMT score distribution shows only a slight increase

301 in the number of samples predicted as epithelial or hybrid E/M in cases of E-cadherin^{high} samples
302 relative to the E-cadherin^{low} samples (**Figure 2E**). Together, using both computational and
303 experimental approaches, our results suggest that E-cadherin overexpression need not be
304 sufficient to induce MET in sarcomas, and that E-cadherin acts independently of
305 migration/invasion programs to inhibit sarcoma aggressiveness.
306
307 E-cadherin suppresses anoikis resistance in sarcomas
308 To explore alternative mechanisms by which E-cadherin may impact the aggressiveness of
309 sarcoma tumors, we analyzed the effect of E-cadherin on anchorage-independent growth. Given
310 the role of E-cadherin as a cell adhesion molecule, we posited that E-cadherin may alter the
311 anoikis resistant phenotype of sarcoma cells. To test this hypothesis, cells expressing an empty
312 vector (EV) or E-cadherin were cultured in soft agar to simulate anchorage-independent growth.
313 Interestingly, E-cadherin expression significantly inhibited the number of colonies formed in soft
314 agar growth assays in 143B cells (**Figure 3A**). This effect was independent of differences in
315 monolayer growth, as E-cadherin expressing cells showed no difference in 2D growth
316 (**Supplementary Figure 1C, F**). We observed similar results in a second sarcoma cell line, RD
317 cells. Ectopic expression of E-cadherin did not induce MET by gene expression, migration, or
318 invasion (**Supplementary Figure 2A-C**). However, consistent with 143B cells, E-cadherin
319 overexpression inhibited anchorage independent growth (**Supplementary Figure 2D**). We next
320 measured spheroid formation to assess the impact of E-cadherin on anchorage-independent
321 growth and morphology. For these experiments, we noted that, despite consistent downregulation
322 of soft agar growth in both RD and 143B cells, E-cadherin was not expressed at the cell
323 membrane of RD cells (**Supplementary Figure 1A**), while E-cadherin was localized at the
324 membrane of 143B cells (**Supplementary Figure 1D**). Because membrane E-cadherin is the
325 most typically-characterized aspect of E-cadherin function, we focused on 143B cells for which
326 E-cadherin was correctly localized to the cell membrane. We also included U2OS cells as a
327 second model for which E-cadherin was localized to the cell membrane (**Supplementary Figure**
328 **1G**). Consistent with our result in soft agar, E-cadherin expressing spheroids formed as tight
329 aggregates and significantly reduced the size of spheroid formation in both 143B and U2OS cells
330 (**Figure 3B, C**). These results indicate that sarcomas with E-cadherin expression have suppressed
331 anoikis resistance as indicated by their deficient ability to grow in anchorage-independent
332 conditions.
333
334 E-cadherin-mediated suppression of anoikis resistance acts, in part, through CREB
335 To determine the signaling pathway(s) through which E-cadherin inhibits anoikis resistance in
336 sarcomas, we performed phospho-kinase arrays on 143B osteosarcoma cells with and without E-
337 cadherin expression. The phospho-kinase arrays contain antibodies against 43 different kinases
338 (R&D Systems). From these arrays, we identified phospho (p)-CREB as consistently
339 downregulated in E-cadherin expressing 143B cells as compared to 143B cells expressing an
340 empty vector lacking E-cadherin (**Figure 4A**). The inhibition of p-CREB in E-cadherin

341 expressing 143B cells was validated by enzyme linked immunosorbent assays (ELISAs) (**Figure**
342 **4B**). Consistent with this, we also observed lower levels of p-CREB in Abrams canine
343 osteosarcoma cells expressing E-cadherin as compared to cells expressing an empty vector
344 lacking E-cadherin (**Figure 4C**).
345 We next asked if E-cadherin-mediated p-CREB inhibition was responsible for the
346 reductions in anchorage-independent growth capacity of E-cadherin expressing cells. To do this,
347 we knocked down CREB using two independent siRNAs and verified knockdown at the mRNA
348 and protein levels in 143B cells, with siRNA_5 providing a stronger knockdown (**Figure 4D, E**).
349 We noted a consistent reduction in soft agar growth with both CREB siRNAs compared to a non-
350 silencing siRNA (**Figure 4F**); however, there was only a significant inhibition of soft agar
351 growth in cells treated with the most effective siRNA_5 (**Figure 4F**). We conclude from these
352 data that downregulation of CREB partially phenocopies E-cadherin expression, although other
353 factors are likely at play in driving anoikis resistance in sarcomas.
354 During our analysis of MET biomarkers and phenotypes in E-cadherin expressing cells,
355 we noted that groups of E-cadherin+ 143B cells lost cell surface N-cadherin expression
356 (**Supplementary Figure 3A**). Interestingly, the reduction in cell surface N-cadherin was not due
357 to changes in N-cadherin expression at either the mRNA or protein levels (**Supplementary**
358 **Figure 3B, C**). Cadherin switching has been observed in carcinomas in which an E-cadherin to
359 N-cadherin switch is prognostic for poorer clinical outcomes (Gravdal et al., 2007; Hazan et al.,
360 2004; Jager et al., 2010). In addition, N-cadherin has been shown to promote anoikis resistance
361 in carcinomas (Ko et al., 2012). Thus, we tested if a reduction of cell surface N-cadherin was
362 responsible for the downregulation of anoikis resistance in E-cadherin+ cells. Knockdown of N-
363 cadherin with two independent siRNAs (**Supplementary Figure 3D**) had no effect on 143B
364 colony formation in soft agar (**Supplementary Figure 3E**). Likewise, N-cadherin knockdown
365 did not alter levels of p-CREB protein, as determined by p-CREB ELISAs (**Supplementary**
366 **Figure 3F**). These results suggest that E-cadherin inhibits anoikis resistance through a pathway
367 that is independent of N-cadherin.
368
369 <u>An E-cadherin/TBX2/CREB axis modulates anchorage-independent growth of sarcomas</u>
370 To elucidate further the signaling axis that modulates E-cadherin/CREB-mediated suppression of
371 anoikis resistance, we investigated additional signaling axes that may be involved with E-
372 cadherin. One of these axes, TBX2, is a transcription factor that can directly repress E-cadherin
373 (Wang et al., 2012), can be modulated by CREB (Liu et al., 2013), and is overexpressed in
374 rhabdomyosarcoma (Zhu et al., 2014, 2016). To determine if E-cadherin regulates TBX2 in
375 sarcomas, we measured levels of TBX2 in E-cadherin expressing 143B cells. TBX2 mRNA was
376 significantly downregulated in E-cadherin+ 143B cells (**Figure 5A**). Similarly, U2OS cells
377 ectopically expressing E-cadherin (**Supplementary Figure 1G**) had significantly lower levels of
378 TBX2 mRNA (**Figure 5B**). To further delineate the directionality of the E-
379 cadherin/CREB/TBX2 signaling network, we performed siRNA-mediated CREB knockdown
380 and measured TBX2 mRNA levels. Interestingly, CREB knockdown had no effect on TBX2

expression (**Figure 5C**), suggesting that CREB is downstream of TBX2 in this gene regulatory network. Consistent with these data, TBX2 knockdown (**Figure 5D**) led to significant reductions in CREB mRNA (**Figure 5E**) and protein (**Figure 5F**). Taken together, these results suggest that E-cadherin inhibits TBX2, which leads to CREB downregulation and suppression of anoikis resistance.

Mathematical modeling of E-cadherin/TBX2 axis regulating anchorage-independent growth

By integrating our quantitative RT-PCR result showing E-cadherin-mediated suppression of TBX2 mRNA with previous reports suggesting E-cadherin to be a transcriptional target of TBX2 (Wang et al., 2012), and regulation of anoikis-related pathways by E-cadherin and/or TBX2 (Kumar et al., 2011; Lingbeek et al., 2002; Zhu et al., 2014), we constructed a mechanism-based mathematical model to decode the dynamics of the E-cadherin/TBX2 axis in mediating anchorage-independent growth **(Figure 6A)**. This model includes the following interactions: (i) mutual repression between E-cadherin and TBX2, (ii) inhibition of NRAGE (neurotrophin receptor-interacting melanoma antigen) by E-cadherin (Kumar et al., 2011), and (iii) inhibition of anoikis by TBX2 complex, which is promoted in the presence of NRAGE (Kumar et al., 2011). Such interconnected regulatory loops can often obviate an intuitive understanding of the emergent outcomes of these interactions (Jolly et al., 2017b). Thus, mechanism-based mathematical models can be a powerful tool for both helping explain previous experimental observations, and for making novel predictions to guide future experimental design (Mobius and Laan, 2015).

Our model predicted that TBX2 knockdown would restrict anchorage-independent growth in a similar way as that by E-cadherin overexpression **(Figure 6B)**. To test this prediction, we used two independent siRNA to TBX2 to knockdown expression and measured anchorage independent growth. Consistent with our prediction, TBX2 knockdown using two independent siRNAs significantly abrogated colony growth in 143B cells **(Figure 6C)**. Further, the model predicted that knockdown of TBX2 under ectopic expression of E-cadherin accentuates anoikis sensitivity **(Figure 6B)**. However, TBX2 knockdown had no effect on spheroid formation, when E-cadherin was overexpressed in U2OS cells **(Figure 6D)**.

The inconsistency in model predictions vs. experimental observations drew our attention to multiple underlying assumptions of the mathematical model – (a) TBX2-mediated inhibition of E-cadherin affects both mRNA and protein levels of E-cadherin, (b) endogenous production of E-cadherin is enough to inhibit TBX2. The first assumption is based on observations in breast epithelial cells MCF10A (Wang et al., 2012); similarly, the second assumption also is likely to be more typical of carcinomas than of sarcomas. Given that our model was constructed using data exclusively taken from carcinomas, we reasoned that the discrepancy between the model and the experimental validation may be due to differences in regulatory networks between carcinomas and sarcomas. Therefore, to determine if similar regulatory networks between TBX2 and E-cadherin exist in sarcomas, we knocked down TBX2 with two independent siRNAs in U2OS cells and measured E-cadherin mRNA and protein levels. TBX2 knockdown led to a

421 modest, albeit significant, two- to four-fold upregulation of E-cadherin mRNA levels **(Figure**
422 **6E)**. More importantly, this modest change in expression in a cell line with relatively low levels
423 of E-cadherin mRNA expression at baseline was not enough of an increase in mRNA to show a
424 change at the protein level **(Figure 6F)**. The relative lack of E-cadherin re-activation upon TBX2
425 knockdown led us to hypothesize that sarcoma cells had alterations in the promoter of E-cadherin
426 that prevented robust increases in expression upon TBX2 downregulation. Consistent with this
427 hypothesis, analysis of sarcoma tumors from The Cancer Genome Atlas (TCGA) revealed that
428 the E-cadherin promoter was significantly more methylated in sarcomas as compared to that in
429 carcinomas **(Figure 6G)**. Moreover, the degree of E-cadherin promoter methylation was lowest
430 in synovial sarcoma (**Figure 6H**), which corresponded with a relative increase in E-cadherin
431 expression (**Figure 6I**). Interestingly, synovial sarcoma often displays epithelioid histological
432 features, including E-cadherin upregulation. This suggests that one potential difference between
433 the E-cadherin/TBX2 axis in sarcomas vs. carcinomas is the ability of TBX2 to access the E-
434 cadherin promoter, which may impact the mathematical models of networks based from largely
435 studies in carcinoma models. Incorporating this new experimental data, we revised our
436 mathematical model to include a weaker inhibition of E-cadherin by TBX2. The revised model
437 predicted that, consistent with our experimental results, the effect of TBX2 knockdown on
438 anoikis sensitivity in the context of E-cadherin overexpression was reduced (**Supplementary**
439 **Figure 4**).
440
441 <u>A mechanical model relates E-cadherin mediated cell-cell adhesion to spheroid formation</u>
442 Our experimental results suggest E-cadherin inhibits soft agar colony formation mediated by
443 suppression of CREB and TBX2 in sarcoma cells. Interestingly, E-cadherin expression alone is
444 sufficient to suppress the size of spheroid formation while TBX2 has no effect on spheroid
445 growth **(Figure 6D)**. The differences in response between these phenotypic assays suggest that
446 E-cadherin may act through different molecular mechanisms to suppress anoikis resistance and
447 spheroid growth. Given the well-described role for E-cadherin as an adhesion molecule, we
448 hypothesized that E-cadherin can regulate spheroid formation through its mechanical role as a
449 regulator of cell-cell adhesion. Indeed, E-cadherin mediated cell-cell adhesion has been proposed
450 to be crucial in mediating formation of cohesive multicellular units such as tumor emboli and
451 invasive collective migration in breast cancer (Elisha et al., 2018; Jolly et al., 2017a; Shamir and
452 Ewald, 2015; Shamir et al., 2014). Consistent with this, U2OS cells overexpressing E-cadherin
453 formed tight multicellular clusters at 24 hours of spheroid formation as compared to control cells
454 **(Figure 7A)**.
455 To quantitatively capture the relationship between cell-cell adhesion and spheroid size,
456 we developed a two-dimensional mechanical model of sphere formation. This model represents
457 each cell by two subcellular elements connected to each other with a contractile force, and
458 incorporates various interconnected biomechanical aspects of cellular aggregation, such as
459 intracellular contraction, intercellular adhesion, cell proliferation, self-propulsion forces of the
460 cells, and friction between the cells and the substrate (Basan et al., 2013; Yang and Levine, 2018;

461 Zimmermann et al., 2016). We initialized our simulations with a seed colony of 233 cells
462 arranged as a two-dimensional circular sheet, and simulated the colony growth for varying levels
463 of intercellular adhesion, while keeping all other parameters the same. The intercellular
464 interaction is repulsive at short distances, attractive at longer distances and becomes zero further
465 away, which models the volume exclusion and cell-cell adhesion. For different levels of
466 adhesion, the attractive part of the intercellular force follows different curves **(Figure 7B)**. This
467 mechanical model predicts a decrease in final spheroid size and the total number of cells with an
468 increase in E-cadherin levels **(Figure 7C)**, and a concomitant increase in cell density
469 **(Supplementary Figure 5)**. Thus, the model predicts that cell-cell adhesion can regulate colony
470 size through mechanical factors.
471 To test if E-cadherin modulates cell-cell adhesion in sarcomas, we quantified the
472 numbers of single cells and cellular aggregates (two or more cells clumped together) using cell-
473 cell adhesion assays for both 143B and U2OS cells upon ectopic expression of an empty vector
474 or E-cadherin. Consistent with our model, we observed that E-cadherin overexpression drives a
475 significant enrichment of multicellular aggregates in both 143B and U2OS cells **(Figure 7D-E),**
476 suggesting that E-cadherin levels can play a fundamental role in enabling cell-cell adhesion in
477 sarcomas. Together, our results integrating gene regulatory network models, mechanical models,
478 and experimental validations indicate that E-cadherin plays a dual role in suppressing sarcoma
479 aggression that is independent of EMT through both signaling-related inhibition of anoikis
480 resistance and mechanics-based inhibition of spheroid formation.
481
482 **Discussion**
483
484 Our integrated computational-experimental study illustrates that E-cadherin inhibits sarcoma
485 aggressiveness in at least the following two ways: first, by inducing anoikis sensitivity through a
486 CREB/TBX2 signaling axis; and second, by increasing cell-cell adhesion and restricting spheroid
487 growth. Anoikis – a Greek word for 'homelessness' – is a specific form of programmed cell
488 death that occurs when cells detach from the extracellular matrix (ECM). Although normal cells
489 require attachment to the ECM to receive cell survival signals, cancer cells overcome the death
490 signals that are driven by loss of cell-ECM attachment (Paoli et al., 2013). Thus, failure to
491 undergo anoikis can lead to anchorage-independent survival of otherwise adherent cells,
492 including at sites where a unique ECM composition prevents cellular attachment (Paoli et al.,
493 2013). Anoikis resistance has, therefore, emerged as a hallmark of cancer and a contributor to
494 metastatic growth (Simpson et al., 2008; Taddei et al., 2012). Interestingly, anoikis has often
495 been studied in the context of EMT in multiple epithelial cancers (Frisch et al., 2013; Huang et
496 al., 2013; Xu et al., 2014); however, ours is among the minority of studies connecting E-cadherin
497 with anoikis sensitivity in sarcomas. Indeed, our results pinpoint an E-cadherin/p-CREB/TBX2
498 axis that mediates anoikis resistant growth in sarcoma cells. This signaling axis is independent of
499 MET, as neither ectopic E-cadherin expression nor TBX2 knockdown had any effect on MET
500 markers in 143B or RD cells. This observation reinforces previous results that overexpression of

transcription factor GRHL2 – an activator of E-cadherin – was sufficient to induce MET in breast cancer cells having undergone EMT, but not in sarcoma (Cieply et al., 2012; Somarelli et al., 2016). Highly methylated promoters of both E-cadherin (**Figure 6D**) and GRHL2 (Somarelli et al., 2016) in sarcomas relative to carcinomas, as observed from analysis of TCGA data, can potentially explain this difference. In this scenario, epigenetic silencing of epithelial promoters would prevent lineage reprogramming and MET. However, it is possible that some sarcoma subtypes are more likely to undergo MET; for instance, E-cadherin expression (**Supplementary Figure 1A**), and an epithelial-like phenotype in general (Yang et al., 2010), appears to be more frequently upregulated in certain soft tissue sarcoma subtypes, such as synovial sarcomas, undifferentiated pleiomorphic sarcomas, and leiomyosarcomas (**Figure 6I**).

While E-cadherin inhibits anoikis resistance through a signaling axis, the role of E-cadherin in suppressing spheroid growth is mediated, at least in part, through its mechanical activity of increasing cell-cell adhesion and cellular aggregation (**Figure 7**). This observation is consistent with previous reports in which knock down of E-cadherin led to less cell-cell adhesion and lower multicellular aggregation in colorectal cancer cells (Stadler et al., 2018). However, unlike our study, this study in colorectal cancer also found that E-cadherin loss led to increased migration and invasion. Yet, despite the fact that E-cadherin did not change migration or invasion in sarcomas, E-cadherin may still inhibit invasiveness of some tumors not by maintaining an epithelial state, but by increasing cell-cell adhesion. In this way, E-cadherin would indirectly reduce invasion by preventing cells from detaching from the bulk tumor without changing the EMT factors involved in migration and/or invasion.

The signaling and mechanical modes of action we observed in suppressing anoikis resistance and spheroid formation, respectively, need not be independent of each other, especially given the interconnections among mechanosensitive and biochemical signaling pathways. For instance, Notch signaling can be mechanosensitive (Riahi et al., 2015), give rise to multiple multicellular patterns of cells in varying phenotypic states (Boareto et al., 2016; Sprinzak et al., 2010), and be involved in anoikis (Stylianou et al., 2006). Similarly, E-cadherin can sense and provide mechanical cues for epithelial homeostasis and collective cell migration (De Beco et al., 2015; Cai et al., 2014; Le Duc et al., 2010). Future studies will be aimed at elucidating the crosstalk between inter-cellular mechano-sensitive and intra-cellular p-CREB/TBX2 modules to yield new insights into the mechanisms underlying non-cell autonomous control of anoikis, as recently observed (Kim et al., 2016). Moreover, it would be intriguing to compare the results for soft agar colony growth and spheroid formation assays for RD cells where E-cadherin exerts an effect on anchorage-independent growth in the absence of membrane localization.

Overall, our results provide a mechanistic basis for the observation that E-cadherin is a prognostic biomarker for improved clinical outcomes in sarcomas. Although E-cadherin upregulation in the clinical setting is likely to be a harbinger of a broader change in EMT/MET programs, our data argue that E-cadherin upregulation also has important effects on sarcoma aggressiveness that are independent of MET induction. Together, these results indicate that

541 targeting the EMT/MET axis in sarcomas may have multiple benefits, including downregulation
542 of stemness, migration, invasion, and anoikis resistance pathways. One way this might be
543 achieved is through epigenetic reprogramming. Indeed, multiple reports in carcinomas suggest
544 that treatment with epigenetic modifiers, including histone deacetylases inhibitors, can
545 upregulate E-cadherin (Choi et al., 2016; Kim et al., 2011; Law et al., 2013; Mateen et al., 2013).
546 Consistent with this hypothesis, when anchorage-dependent and anchorage-independent
547 subpopulations of osteosarcoma cells are compared, the anchorage-independent subpopulations
548 are significantly more susceptible to epigenetic modifying therapies (Foley et al., 2015). A
549 similar strategy could be used to drive sarcomas toward a more epithelial-like phenotype and
550 lower their aggressiveness by targeting many aggressive phenotypes simultaneously. Such
551 combinatorial therapies may limit the adaptive phenotypic plasticity of cancer cells – a crucial
552 determinant of therapeutic resistance (Jolly et al., 2018).
553

554 **Acknowledgments**

555 The results published here are in part based upon data generated by the TCGA Research
556 Network: http://cancergenome.nih.gov. The authors acknowledge the Duke University Cell
557 Culture Facility and the Duke Cancer Institute Flow Cytometry Shared Resource. HL was
558 supported by NSF Center for Theoretical Biological Physics (NSF PHY-1427654) and NSF
559 DMS-1361411, and as a CPRIT (Cancer Prevention and Research Institute of Texas) Scholar in
560 Cancer Research of the State of Texas at Rice University. MKJ received a training fellowship
561 from the Gulf Coast Consortia on the Computational Cancer Biology Training Program (CPRIT
562 grant no. RP170593). KEW was supported by the NIH F32 CA192630. JAS wishes to
563 acknowledge support from Meg and Bill Lindenberger, the Paul and Shirley Friedland Fund, the
564 Triangle Center for Evolutionary Medicine, and funds raised in memory of Muriel E.
565 Rudershausen (riding4research.org).
566

567 **References**

568 Basan, M., Elgeti, J., Hannezo, E., Rappel, W.-J.W.-J., and Levine, H. (2013). Alignment of
569 cellular motility forces with tissue flow as a mechanism for efficient wound healing. Proc. Natl.
570 Acad. Sci. U. S. A. *110*, 2452–2459.

571 De Beco, S., Perney, J.B., Coscoy, S., and Amblard, F. (2015). Mechanosensitive adaptation of
572 E-cadherin turnover across adherens junctions. PLoS One *10*, 1–14.

573 Boareto, M., Jolly, M.K., Goldman, A., Pietilä, M., Mani, S.A., Sengupta, S., Ben-Jacob, E.,
574 Levine, H., and Onuchic, J.N. (2016). Notch-Jagged signalling can give rise to clusters of cells
575 exhibiting a hybrid epithelial/mesenchymal phenotype. J. R. Soc. Interface *13*, 20151106.

576 Brown, R.L., Reinke, L.M., Damerow, M.S., Perez, D., Chodosh, L. a., Yang, J., and Cheng, C.
577 (2011). CD44 splice isoform switching in human and mouse epithelium is essential for
578 epithelial-mesenchymal transition and breast cancer progression. J. Clin. Invest. *121*, 1064–1074.

579 Cai, D., Chen, S.C., Prasad, M., He, L., Wang, X., Choesmel-Cadamuro, V., Sawyer, J.K.,
580 Danuser, G., and Montell, D.J. (2014). Mechanical feedback through E-cadherin promotes

581 direction sensing during collective cell migration. Cell *157*, 1146–1159.

582 Chao, Y.L., Shepard, C.R., and Wells, A. (2010). Breast carcinoma cells re-express E-cadherin
583 during mesenchymal to epithelial reverting transition. Mol. Cancer *9*, 179.

584 Chen, W., and Obrink, B. (1991). Cell-cell contacts mediated by E-cadherin (uvomorulin)
585 restrict invasive behavior of L-cells. J. Cell Biol. *114*, 319–327.

586 Chen, A., Beetham, H., Black, M.A., Priya, R., Telford, B.J., Guest, J., Wiggins, G.A.R.,
587 Godwin, T.D., Yap, A.S., and Guilford, P.J. (2014). E-cadherin loss alters cytoskeletal
588 organization and adhesion in non-malignant breast cells but is insufficient to induce an
589 epithelial-mesenchymal transition. BMC Cancer *14*, 552.

590 Choi, S.Y., Kee, H.J., Kurz, T., Hansen, F.K., Ryu, Y., Kim, G.R., Lin, M.Q., Jin, L., Piao, Z.H.,
591 and Jeong, M.H. (2016). Class I HDACs specifically regulate E-cadherin expression in human
592 renal epithelial cells. J. Cell. Mol. Med. *20*, 2289–2298.

593 Cieply, B., Riley IV, P., Pifer, P.M., Widmeyer, J., Addison, J.B., Ivanov, A. V., Denvir, J., and
594 Frisch, S.M. (2012). Suppression of the epithelial-mesenchymal transition by grainyhead-like-2.
595 Cancer Res. *72*, 2440–2453.

596 Corso, G., Intra, M., Trentin, C., Veronesi, P., and Galimberti, V. (2016). CDH1 germline
597 mutations and hereditary lobular breast cancer. Fam. Cancer *15*, 215–219.

598 De Craene, B., and Berx, G. (2013). Regulatory networks defining EMT during cancer initiation
599 and progression. Nat. Rev. Cancer *13*, 97–110.

600 Le Duc, Q., Shi, Q., Blonk, I., Sonnenberg, A., Wang, N., Leckband, D., and De Rooij, J. (2010).
601 Vinculin potentiates E-cadherin mechanosensing and is recruited to actin-anchored sites within
602 adherens junctions in a myosin II-dependent manner. J. Cell Biol. *189*, 1107–1115.

603 Elisha, Y., Kalchenko, V., Kuznetsov, Y., and Geiger, B. (2018). Dual role of E-cadherin in the
604 regulation of invasive collective migration of mammary carcinoma cells. Sci. Rep. *8*, 4986.

605 Foley, J.M., Scholten, D.J., Monks, N.R., Cherba, D., Monsma, D.J., Davidson, P., Dylewski, D.,
606 Dykema, K., Winn, M.E., and Steensma, M.R. (2015). Anoikis-resistant subpopulations of
607 human osteosarcoma display significant chemoresistance and are sensitive to targeted epigenetic
608 therapies predicted by expression profiling. J. Transl. Med. *13*, 110.

609 Frisch, S.M., Schaller, M., and Cieply, B. (2013). Mechanisms that link the oncogenic epithelial–
610 mesenchymal transition to suppression of anoikis. J. Cell Sci. *126*, 21–29.

611 Gravdal, K., Halvorsen, O.J., Haukaas, S.A., and Akslen, L.A. (2007). A switch from E-cadherin
612 to N-cadherin expression indicates epithelial to mesenchymal transition and is of strong and
613 independent importance for the progress of prostate cancer. Clin. Cancer Res. *13*, 7003–7011.

614 Guilford, P., Hopkins, J., Harraway, J., McLeod, M., McLeod, N., Harawira, P., Taite, H.,
615 Scoular, R., Miller, A., and Reeve, a E. (1998). E-cadherin germline mutations in familial
616 gastric cancer. Nature *392*, 402–405.

617 Hazan, R.B., Qiao, R., Keren, R., Badano, I., and Suyama, K. (2004). Cadherin switch in tumor
618 progression. Ann. N. Y. Acad. Sci. *1014*, 155–163.

619 De Herreros, A.G., Peiró, S., Nassour, M., and Savagner, P. (2010). Snail family regulation and
620 epithelial mesenchymal transitions in breast cancer progression. J. Mammary Gland Biol.
621 Neoplasia *15*, 135–147.

622 Hong, S.-M., Li, A., Olino, K., Wolfgang, C.L., Herman, J.M., Schulick, R.D., Iacobuzio-
623 Donahue, C., Hruban, R.H., and Goggins, M. (2011). Loss of E-cadherin expression and
624 outcome among patients with resectable pancreatic adenocarcinomas. Mod. Pathol. *24*, 1237–
625 1247.

626 Huang, R.Y.-J., Wong, M.K., Tan, T.Z., Kuay, K.T., Ng, a H.C., Chung, V.Y., Chu, Y.-S.,
627 Matsumura, N., Lai, H.-C., Lee, Y.F., et al. (2013). An EMT spectrum defines an anoikis-
628 resistant and spheroidogenic intermediate mesenchymal state that is sensitive to e-cadherin
629 restoration by a src-kinase inhibitor, saracatinib (AZD0530). Cell Death Dis. *4*, e915.

630 Jager, T., Becker, M., Eisenhardt, A., Tilki, D., Totsch, M., Schmid, K.W., Romics, I., Rubben,
631 H., Ergun, S., and Szarvas, T. (2010). The prognostic value of cadherin switch in bladder cancer.
632 Oncol. Rep. *23*, 1125–1132.

633 Jia, D., Jolly, M.K., Tripathi, S.C., Hollander, P. Den, Huang, B., Lu, M., Celiktas, M., Ramirez-
634 Pena, E., Ben-Jacob, E., Onuchic, J.N., et al. (2017). Distinguishing Mechanisms Underlying
635 EMT Tristability. Cancer Converg. *1*, 2.

636 Jin, L., Li, D., Lee, J.S., Elf, S., Alesi, G.N., Fan, J., Kang, H.-B., Wang, D., Fu, H., Taunton, J.,
637 et al. (2013). p90 RSK2 mediates antianoikis signals by both transcription-dependent and -
638 independent mechanisms. Mol. Cell. Biol. *33*, 2574–2585.

639 Jolly, M.K., Boareto, M., Debeb, B.G., Aceto, N., Farach-Carson, M.C., Woodward, W.A., and
640 Levine, H. (2017a). Inflammatory Breast Cancer: a model for investigating cluster-based
641 dissemination. NPJ Breast Cancer *3*, 21.

642 Jolly, M.K., Tripathi, S.C., Somarelli, J.A., Hanash, S.M., and Levine, H. (2017b).
643 Epithelial/mesenchymal plasticity: how have quantitative mathematical models helped improve
644 our understanding? Mol. Oncol. *11*, 739–754.

645 Jolly, M.K., Ware, K.E., Gilja, S., Somarelli, J.A., and Levine, H. (2017c). EMT and MET:
646 necessary or permissive for metastasis? Mol. Oncol. *11*, 755–769.

647 Jolly, M.K., Kulkarni, P., Weninger, K., Orban, J., and Levine, H. (2018). Phenotypic plasticity,
648 bet-hedging, and androgen independence in prostate cancer: Role of non-genetic heterogeneity.
649 Front. Oncol. *8*, 50.

650 Kang, H.G., Jenabi, J.M., Zhang, J., Keshelava, N., Shimada, H., May, W.A., Ng, T., Reynolds,
651 C.P., Triche, T.J., and Sorensen, P.H.B. (2007). E-cadherin cell-cell adhesion in Ewing tumor
652 cells mediates suppression of anoikis through activation of the ErbB4 tyrosine kinase. Cancer
653 Res. *67*, 3094–3105.

654 Kim, N.H., Kim, S.N., and Kim, Y.K. (2011). Involvement of HDAC1 in E-cadherin expression

655 in prostate cancer cells; its implication for cell motility and invasion. Biochem. Biophys. Res.
656 Commun. *404*, 915–921.

657 Kim, S.Y., Hong, S.H., Basse, P.H., Wu, C., Bartlett, D.L., Kwon, Y.T., and Lee, Y.J. (2016).
658 Cancer Stem Cells Protect Non-Stem Cells From Anoikis: Bystander Effects. J. Cell. Biochem.
659 *2301*, 2289–2301.

660 Ko, H., Kim, S., Jin, C.-H., Lee, E., Ham, S., Yook, J.I., and Kim, K. (2012). Protein Kinase
661 Casein Kinase 2-Mediated Upregulation of N-Cadherin Confers Anoikis Resistance on
662 Esophageal Carcinoma Cells. Mol. Cancer Res. *10*, 1032–1038.

663 Kuijjer, M.L., Rydbeck, H., Kresse, S.H., Buddingh, E.P., Lid, A.B., Roelofs, H., Burger, H.,
664 Myklebost, O., Hogendoorn, P.C.W., Meza-Zepeda, L.A., et al. (2012). Telomerase Activity is a
665 Biomarker for High Grade Malignant Peripheral Nerve Sheath Tumors in Neurofibromatosis
666 Type 1 Individuals. Genes. Chromosomes Cancer *51*, 696–706.

667 Kumar, S., Park, S.H., Cieply, B., Schupp, J., Killiam, E., Zhang, F., Rimm, D.L., and Frisch,
668 S.M. (2011). A Pathway for the Control of Anoikis Sensitivity by E-Cadherin and Epithelial-to-
669 Mesenchymal Transition. Mol. Cell. Biol. *31*, 4036–4051.

670 Law, M.E., Corsino, P.E., Jahn, S.C., Davis, B.J., Chen, S., Patel, B., Pham, K., Lu, J., Sheppard,
671 B., Nørgaard, P., et al. (2013). Glucocorticoids and histone deacetylase inhibitors cooperate to
672 block the invasiveness of basal-like breast cancer cells through novel mechanisms. Oncogene *32*,
673 1316–1329.

674 Lewis, J.E., Jensen, P.J., Johnson, K.R., and Wheelock, M.J. (1995). E-cadherin mediates
675 adherens junction organization through protein kinase C. J. Cell Sci. *107*, 3615–3621.

676 Li, Z., Yin, S., Zhang, L., Liu, W., and Chen, B. (2017). Prognostic value of reduced E-cadherin
677 expression in breast cancer: a meta-analysis. Oncotarget *8*, 16445–16455.

678 Lingbeek, M.E., Jacobs, J.J.L., and Van Lohuizen, M. (2002). The T-box repressors TBX2 and
679 TBX3 specifically regulate the tumor suppressor gene p14ARF via a variant T-site in the
680 initiator. J. Biol. Chem. *277*, 26120–26127.

681 Liu, F., Cao, J., Lv, J., Dong, L., Pier, E., Xu, G.X., Wang, R., Xu, Z., Goding, C., and Cui, R.
682 (2013). TBX2 expression is regulated by PAX3 in the melanocyte lineage. Pigment Cell
683 Melanoma Res *26*, 67–77.

684 Lu, M., Jolly, M.K., Levine, H., Onuchic, J.N., and Ben-Jacob, E. (2013). MicroRNA-based
685 regulation of epithelial–hybrid–mesenchymal fate determination. Proc. Natl. Acad. Sci. *110*,
686 18144–18149.

687 Mateen, S., Raina, K., Agarwal, C., Chan, D., and Agarwal, R. (2013). Silibinin synergizes with
688 histone deacetylase and DNA methyltransferase inhibitors in upregulating E-cadherin expression
689 together with inhibition of migration and invasion of human non-small cell lung cancer cells. J
690 Pharmacol Exp Ther *345*, 206–214.

691 Mobius, W., and Laan, L. (2015). Physical and Mathematical Modeling in Experimental Papers.
692 Cell *163*, 1577–1583.

693 Nieto, M.A., Huang, R.Y., Jackson, R.A., and Thiery, J.P. (2016). EMT: 2016. Cell *166*, 21–45.

694 Orsulic, S., Huber, O., Aberle, H., Arnold, S., and Kemler, R. (1999). E-cadherin binding
695 prevents beta-catenin nuclear localization and beta-catenin/LEF-1-mediated transactivation. J.
696 Cell Sci. *112*, 1237–1245.

697 Palorini, R., Votta, G., Pirola, Y., De Vitto, H., De Palma, S., Airoldi, C., Vasso, M.,
698 Ricciardiello, F., Lombardi, P.P., Cirulli, C., et al. (2016). Protein Kinase A Activation Promotes
699 Cancer Cell Resistance to Glucose Starvation and Anoikis. PLoS Genet. *12*, e1005931.

700 Paoli, P., Giannoni, E., and Chiarugi, P. (2013). Anoikis molecular pathways and its role in
701 cancer progression. Biochim. Biophys. Acta - Mol. Cell Res. *1833*, 3481–3498.

702 Riahi, R., Sun, J., Wang, S., Long, M., Zhang, D.D., and Wong, P.K. (2015). Notch1-Dll4
703 signalling and mechanical force regulate leader cell formation during collective cell migration.
704 Nat. Commun. *6*, 6656.

705 Richards, F.M., McKee, S.A., Rajpar, M.H., Cole, T.R.P., Evans, D.G.R., Jankowski, J.A.,
706 McKeown, C., Sanders, D.S.A., and Maher, E.R. (1999). Germline E-cadherin gene (CDH1)
707 mutations predispose to familial gastric cancer and colorectal cancer. Hum. Mol. Genet. *8*, 607–
708 610.

709 Schmalhofer, O., Brabletz, S., and Brabletz, T. (2009). E-cadherin, beta-catenin, and ZEB1 in
710 malignant progression of cancer. Cancer Metastasis Rev. *28*, 151–166.

711 Shamir, E.R., and Ewald, A.J. (2015). Adhesion in mammary development: novel roles for E-
712 cadherin in individual and collective cell migration. Curr Top Dev Biol *112*, 353–382.

713 Shamir, E.R., Pappalardo, E., Jorgens, D.M., Coutinho, K., Tsai, W.T., Aziz, K., Auer, M., Tran,
714 P.T., Bader, J.S., and Ewald, A.J. (2014). Twist1-induced dissemination preserves epithelial
715 identity and requires E-cadherin. J. Cell Biol. *204*, 839–856.

716 Siegel, R., Miller, K., and Jemal, A. (2017). Cancer statistics , 2017 . CA Cancer J Clin *67*, 7–30.

717 Simpson, C.D., Anyjwe, K., and Schimmer, A.D. (2008). Anoikis resistance and tumor
718 metastasis. Cancer Lett. *272*, 177–185.

719 Somarelli, J.A., Shetler, S., Jolly, M.K., Wang, X., Bartholf Dewitt, S., Hish, A.J., Gilja, S.,
720 Eward, W.C., Ware, K.E., Levine, H., et al. (2016). Mesenchymal-epithelial transition in
721 sarcomas is controlled by the combinatorial expression of microRNA 200s and GRHL2. Mol.
722 Cell. Biol. *36*, 2503–2513.

723 Sprinzak, D., Lakhanpal, A., Lebon, L., Santat, L.A., Fontes, M.E., Anderson, G.A., Garcia-
724 Ojalvo, J., and Elowitz, M.B. (2010). Cis-interactions between Notch and Delta generate
725 mutually exclusive signalling states. Nature *465*, 86–90.

726 Stadler, M., Scherzer, M., Walter, S., Holzner, S., Pudelko, K., Riedl, A., Unger, C., Kramer, N.,
727 Weil, B., Neesen, J., et al. (2018). Exclusion from spheroid formation identifies loss of essential
728 cell-cell adhesion molecules in colon cancer cells. Sci. Rep. *8*, 1151.

729 Stylianou, S., Clarke, R.B., and Brennan, K. (2006). Aberrant activation of Notch signaling in
730 human breast cancer. Cancer Res. *66*, 1517–1525.

731 Taddei, M.L., Giannoni, E., Fiaschi, T., and Chiarugi, P. (2012). Anoikis: An emerging hallmark
732 in health and diseases. J. Pathol. *226*, 380–393.

733 Tam, W.L., and Weinberg, R.A. (2013). The epigenetics of epithelial-mesenchymal plasticity in
734 cancer. Nat. Med. *19*, 1438–1449.

735 Tian, W., Wang, G., Yang, J., Pan, Y., and Ma, Y. (2013). Prognostic role of E-cadherin and
736 Vimentin expression in various subtypes of soft tissue leiomyosarcomas. Med. Oncol. *30*, 401.

737 Wang, B., Lindley, L.E., Fernandez-Vega, V., Rieger, M.E., Sims, A.H., and Briegel, K.J.
738 (2012). The T box transcription factor TBX2 promotes epithelial-mesenchymal transition and
739 invasion of normal and malignant breast epithelial cells. PLoS One *7*, e41355.

740 Wang, N., He, Y.-L., Pang, L.-J., Zou, H., Liu, C.-X., Zhao, J., Hu, J.-M., Zhang, W.-J., Qi, Y.,
741 and Li, F. (2015a). Down-regulated E-cadherin expression is associated with poor five-year
742 overall survival in bone and soft tissue sarcoma: Results of a meta-analysis. PLoS One *10*,
743 e0121448.

744 Wang, N., He, Y.-L., Pang, L.-J., Zou, H., Liu, C.-X., Zhao, J., Hu, J.-M., Zhang, W.-J., Qi, Y.,
745 and Li, F. (2015b). Down-regulated E-cadherin expression is associated with poor five-year
746 overall survival in bone and soft tissue sarcoma: Results of a meta-analysis. PLoS One *10*,
747 e0121448.

748 Xu, S., Yang, Y., Dong, L., Qiu, W., Yang, L., Wang, X., and Liu, L. (2014). Construction and
749 characteristics of an E-cadherin-related three-dimensional suspension growth model of ovarian
750 cancer. Sci. Rep. *4*, 5646.

751 Yang, J., Eddy, J. a, Pan, Y., Hategan, A., Tabus, I., Wang, Y., Cogdell, D., Price, N.D., Pollock,
752 R.E., Lazar, A.J.F., et al. (2010). Integrated proteomics and genomics analysis reveals a novel
753 mesenchymal to epithelial reverting transition in leiomyosarcoma through regulation of slug.
754 Mol. Cell. Proteomics *9*, 2405–2413.

755 Yin, K., Liao, Q., He, H., and Zhong, D. (2012). Prognostic value of Twist and E-cadherin in
756 patients with osteosarcoma. Med. Oncol. *29*, 3449–3455.

757 Zhu, B., Zhang, M., Byru, S., Tackett, A.J., and Davie, J.K. (2014). TBX2 blocks myogenesis
758 and promotes proliferation in rhabdomyosarcoma cells. Int J Cancer *135*, 785–797.

759 Zhu, B., Zhang, M., Williams, E.M., Keller, C., Mansoor, A., and Davie, J.K. (2016). TBX2
760 represses PTEN in rhabdomyosarcoma and skeletal muscle. Oncogene *35*, 4212–4224.

761 Zimmermann, J., Camley, B.A., Rappel, W.-J., and Levine, H. (2016). Contact inhibition of
762 locomotion determines cell – cell and cell – substrate forces in tissues. Proc. Natl. Acad. Sci.
763 *113*, 2660–2665.

764 Borowicz, S., M. Van Scoyk, S. Avasarala, M. K. Karuppusamy Rathinam, J. Tauler, R. K.
765 Bikkavilli and R. A. Winn (2014). "The soft agar colony formation assay." J Vis Exp(92):
766 e51998.
767
768 George, J. T., M. K. Jolly, S. Xu, J. A. Somarelli and H. Levine (2017). "Survival Outcomes in
769 Cancer Patients Predicted by a Partial EMT Gene Expression Scoring Metric." Cancer Res
770 **77**(22): 6415-6428.
771
772 Gottardi, C. J., E. Wong and B. M. Gumbiner (2001). "E-cadherin suppresses cellular
773 transformation by inhibiting beta-catenin signaling in an adhesion-independent manner." J Cell
774 Biol **153**(5): 1049-1060.
775
776 Kuijjer, M. L., H. Rydbeck, S. H. Kresse, E. P. Buddingh, A. B. Lid, H. Roelofs, H. Burger, O.
777 Myklebost, P. C. Hogendoorn, L. A. Meza-Zepeda and A. M. Cleton-Jansen (2012).
778 "Identification of osteosarcoma driver genes by integrative analysis of copy number and gene
779 expression data." Genes Chromosomes Cancer **51**(7): 696-706.
780
781 Somarelli, J. A., S. Shetler, M. K. Jolly, X. Wang, S. Bartholf Dewitt, A. J. Hish, S. Gilja, W. C.
782 Eward, K. E. Ware, H. Levine, A. J. Armstrong and M. A. Garcia-Blanco (2016).
783 "Mesenchymal-Epithelial Transition in Sarcomas Is Controlled by the Combinatorial Expression
784 of MicroRNA 200s and GRHL2." Mol Cell Biol **36**(19): 2503-2513.
785

786 Yang, Y. and H. Levine (2018). "Role of the supracellular actomyosin cable during epithelial
787 wound healing." Soft Matter.

788

789 **Figure Legends**

790

791 **Figure 1. E-cadherin upregulation is prognostic for improved outcomes in sarcoma. A-B.**
792 Osteosarcomas with elevated E-cadherin have better metastasis-free survival (**A**) and overall
793 survival (**B**) as compared to tumors with low/no E-cadherin expression. **C-D.** Soft tissue
794 sarcomas (STS) from The Cancer Genome Atlas with higher E-cadherin mRNA (**C**) and protein
795 expression (**D**) have improved overall survival as compared to tumors with low or no E-cadherin.

796 **Figure 2. Ectopic E-cadherin expression in sarcoma cells does not alter EMT. A.** E-cadherin
797 expression significantly correlates with the EMT score of sarcoma tumors in The Cancer
798 Genome Atlas. **B.** Ectopic expression of E-cadherin in 143B human osteosarcoma cells has no
799 influence on mesenchymal markers. **C.** E-cadherin expression has no effect on migration of
800 143B cells. Images (left) were collected every two hours and quantified (right) using the
801 IncuCyte Zoom system. **D.** E-cadherin expression does not change invasion in 143B cells. **E.**
802 Empirical probably density functions of EMT scores for CDH1-high (red) and CDH1-low (blue)
803 TCGA Sarcoma sample was constructed by interpolation of the EMT score histogram ($E<0.5$,
804 $0.5 \leq E/M \leq 1.5$, $M>1.5$). EMT score distribution showed no significant difference when separated

805 for E-cadherin^{high} vs. E-cadherin^{low} expression from analysis of publicly-available sarcoma data
806 sets.
807
808 **Figure 3. E-cadherin inhibits anoikis resistance of sarcomas. A.** Anchorage-independent
809 growth of 143B cells expressing E-cadherin was significantly inhibited. **B-C.** E-cadherin
810 expression leads to reduces spheroid size in **C.** 143B and **D.** U2OS cells.
811
812 **Figure 4. Ectopic expression of E-cadherin in sarcoma cells inhibits phospho-CREB levels.**
813 **A.** A phospho-kinase array revealed that E-cadherin led to downregulation of phospho-CREB. **B.**
814 E-cadherin-mediated phospho-CREB inhibition was verified by ELISAs. **C.** Abrams canine
815 osteosarcoma cells exhibited reduced phospho-CREB in E-cadherin over-expressing cells. **D.**
816 QRT-PCR confirmed knockdown of CREB with two independent siRNAs. **E.** Western blotting
817 to confirm knockdown of CREB in 143B cells. **F.** CREB knockdown led to a modest
818 downregulation of 143B colony growth in soft agar.
819
820 **Figure 5. TBX2 knockdown phenocopies E-cadherin-mediated CREB inhibition. A.** TBX2
821 mRNA is downregulated in E-cadherin-expressing **A.** 143B cells and **B.** U2OS cells. **C.** CREB
822 knockdown with two independent siRNAs had no effect on TBX2 mRNA. **D-F.** Conversely,
823 TBX2 knockdown, verified in **D.** led to a significant reduction in CREB mRNA (**E**) and protein
824 level (**F**).
825
826 **Figure 6. E-cad/TBX2 interplay mediates anoikis sensitivity. A.** Intracellular regulatory
827 circuit modulating anoikis sensitivity. **B.** Mathematical model predicts similar effects of Ecad-
828 OE and TBX2-KD in anoikis sensitivity. **C.** TBX2 knockdown using two independent siRNAs
829 inhibited anoikis resistance of 143B cells. **D.** TBX2 downregulation did not affect sphere
830 formation in the presence of ectopic E-cadherin expression**. E.** TBX2 knockdown upregulates E-
831 cadherin mRNA. **F.** Western blot analysis of U2OS cells upon TBX2 knockdown indicates E-
832 cadherin protein is not upregulated by loss of TBX2. Prostate cancer (PC) cell line, LNCaP, was
833 used as a positive control for E-cadherin expression. **G.** The E-cadherin promoter is differentially
834 methylated in sarcomas as compared to carcinomas. **H.** Synovial sarcomas, which often display
835 epithelioid histopathological features, have the lowest levels of E-cadherin promoter methylation
836 of all sarcoma subtypes. **I.** Among soft tissue sarcoma histological subtypes E-cadherin mRNA
837 expression is highest in synovial sarcomas. Letters indicate statistically significant associations
838 between groups.
839
840 **Figure 7. E-cadherin inhibits spheroid formation by increased cell-cell adhesion. A.** E-
841 cadherin causes tighter clustering of cells during spheroid formation. **B.** A mechanical model
842 illustrates the relationship between particle distance to adhesion. **C.** A mechanical model predicts
843 E-cadherin drives down spheroid size through an increase in cell-cell adhesion. **D-E.** As
844 predicted in the model, ectopic E-cadherin expression increases cell-cell adhesion in 143B (**D**)
845 and U2OS (**E**) cells.
846
847
848 **Figures**
849

850 **Figure 1**

851

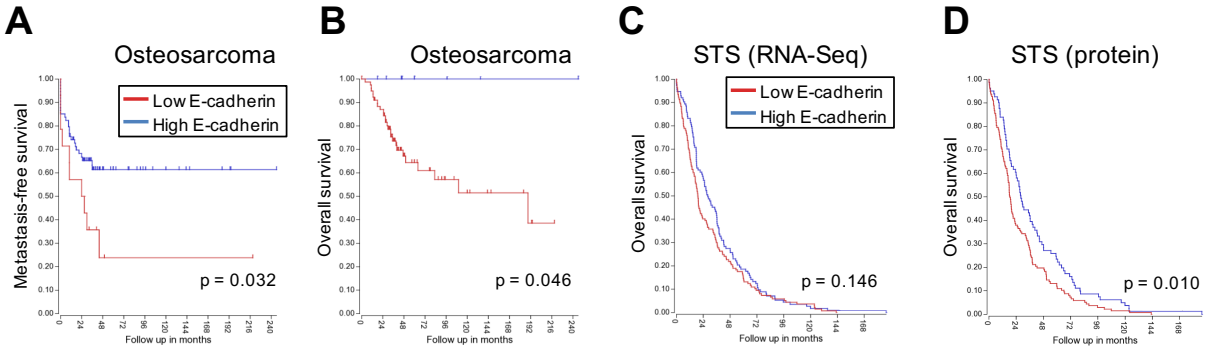

852
853
854
855
856
857
858
859
860
861
862
863
864
865
866
867
868
869
870
871
872
873
874
875
876
877
878
879
880
881
882

883 **Figure 2**

884

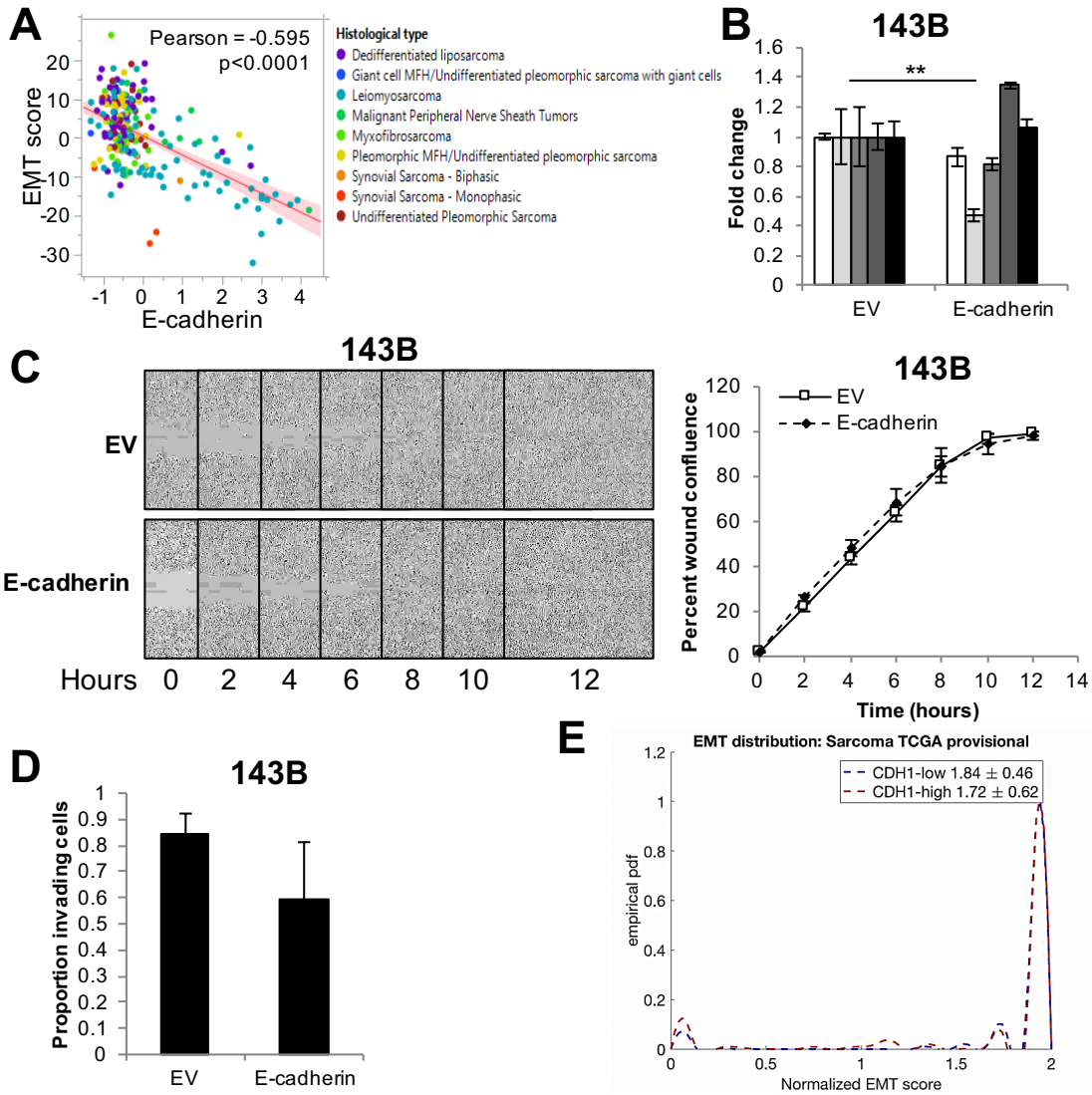

885
886
887
888
889
890
891
892
893
894
895
896
897

898 **Figure 3**

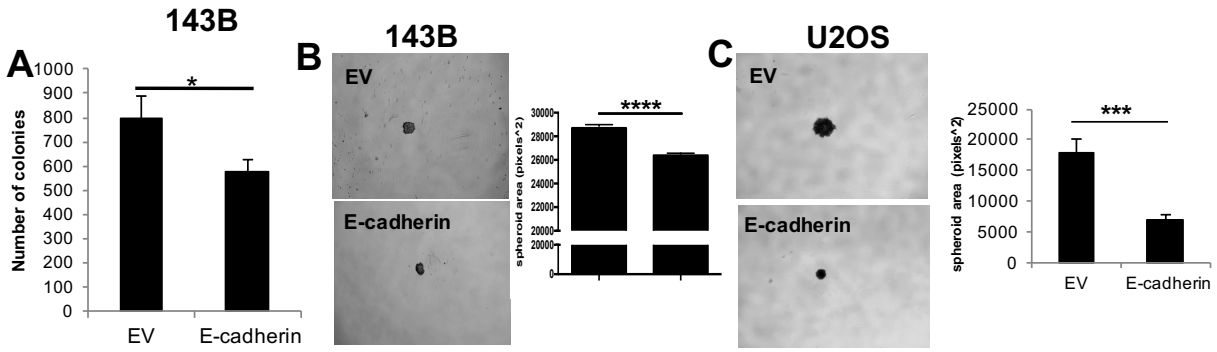

899
900
901
902
903
904
905
906
907
908
909
910
911
912
913
914
915
916
917
918
919
920
921
922
923
924
925
926
927
928
929
930

931 **Figure 4**

932

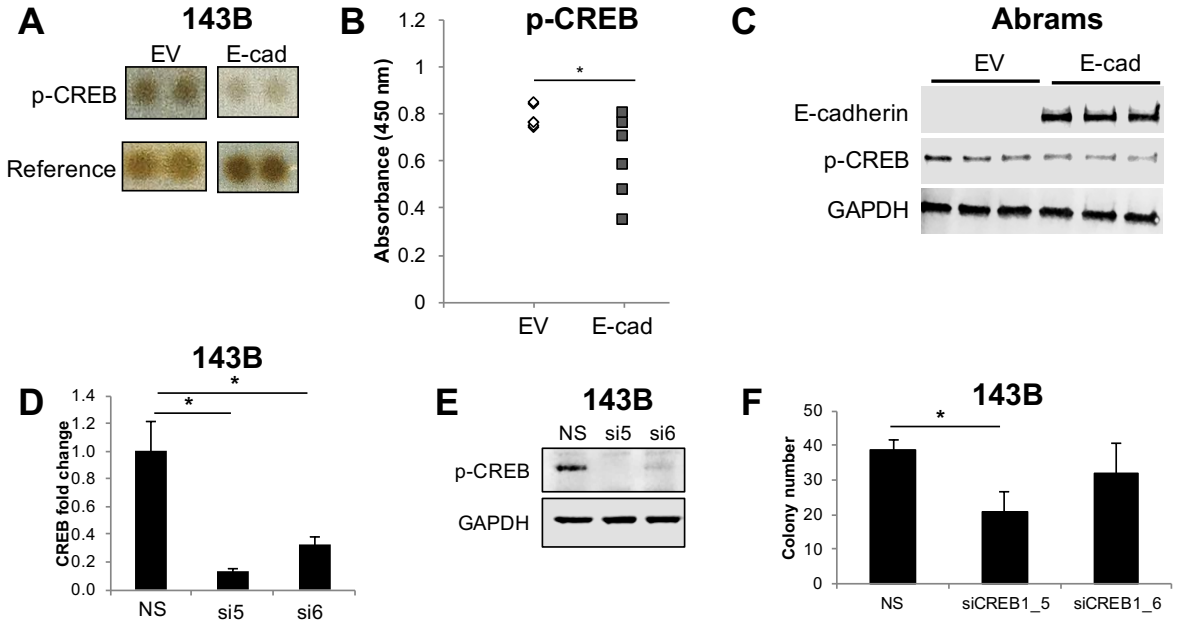

933
934
935
936
937
938
939
940
941
942
943
944
945
946
947
948
949
950
951
952
953
954
955
956

957 **Figure 5**

958

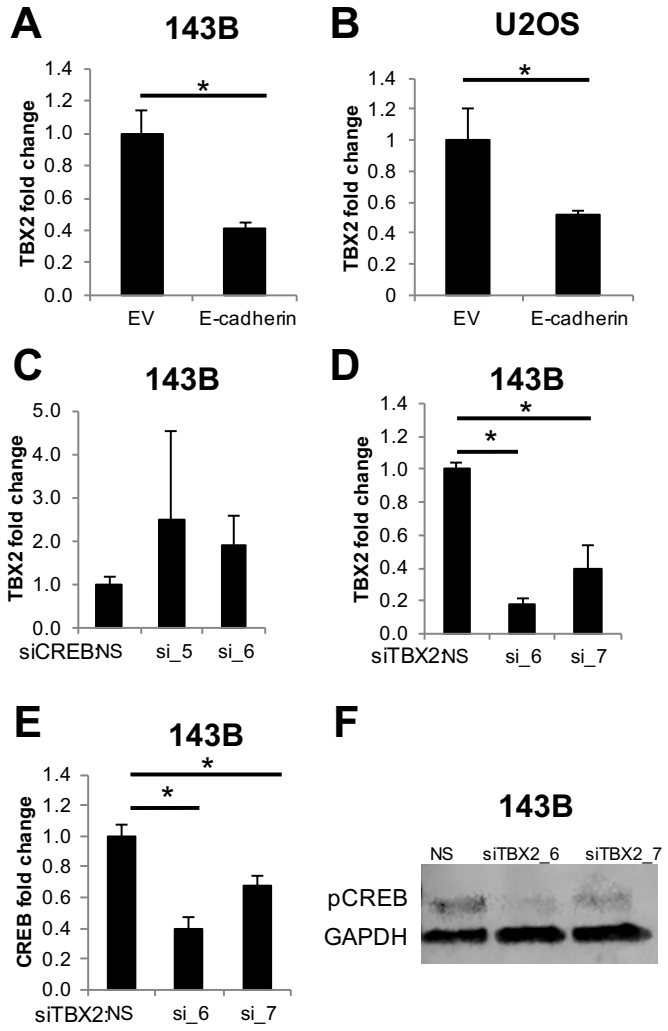

959
960
961
962
963
964
965
966
967
968
969
970
971
972

973 **Figure 6**

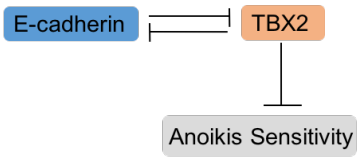

Treatment	FC (Anoikis)
E-cad OE	1.54 +/- 0.02
TBX2 KD	1.54 +/- 0.14
Both	1.89 +/- 0.04

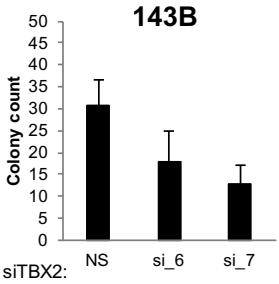

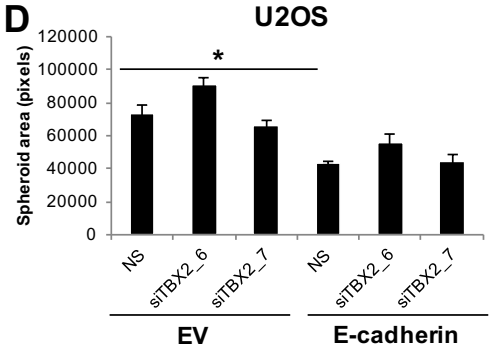

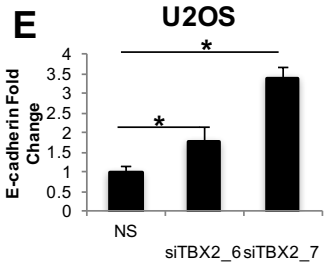

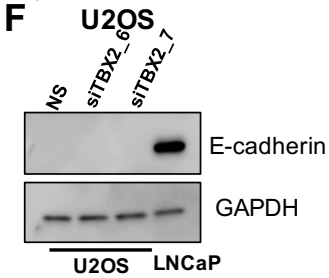

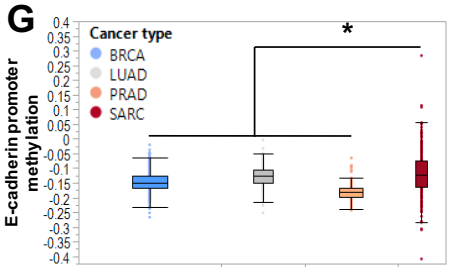

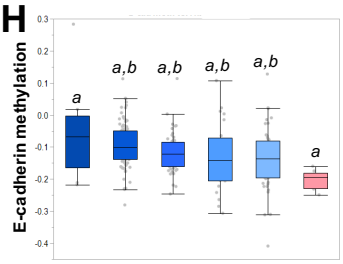

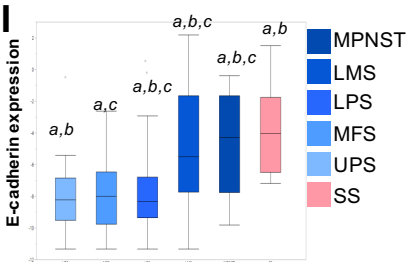

974
975
976
977
978
979
980
981
982
983
984
985
986
987
988
989
990
991
992

Figure 7

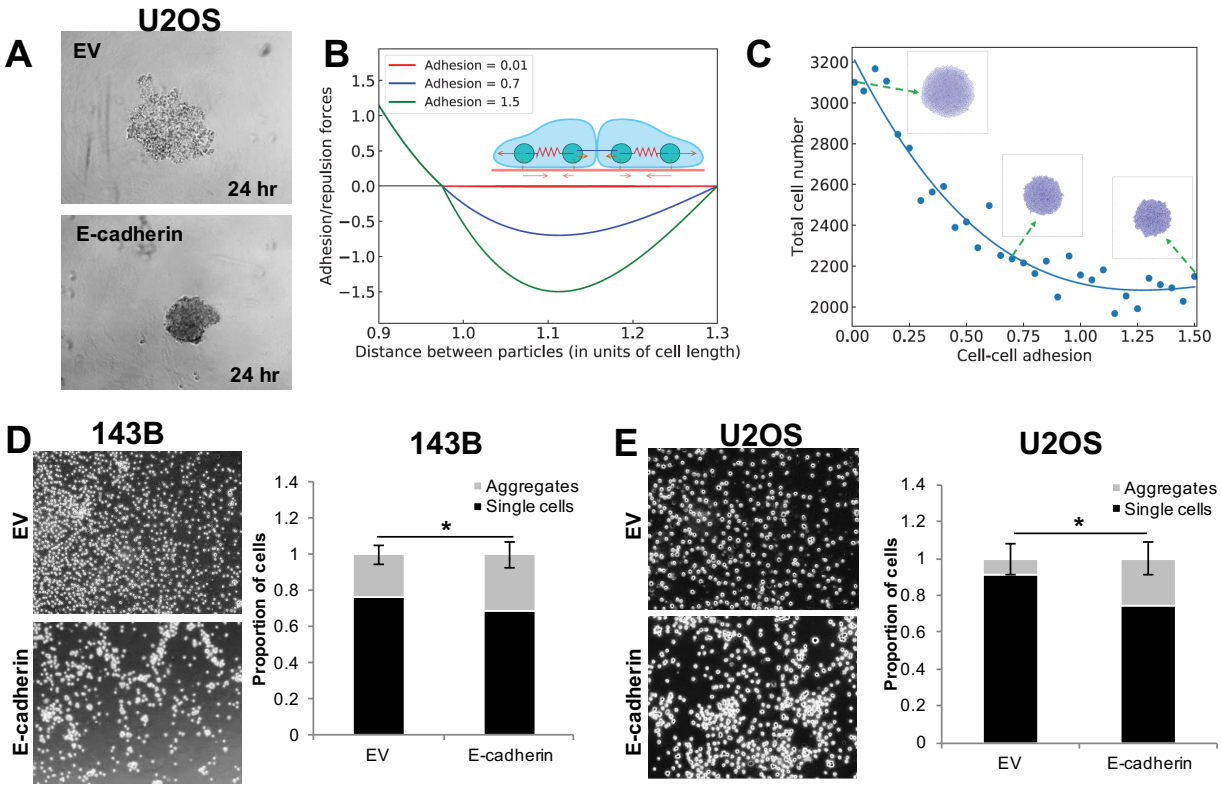
U2OS
A
EV
24 hr
E-cadherin
24 hr
B
Adhesion = 0.01
Adhesion = 0.7
Adhesion = 1.5
Adhesion/repulsion forces
Distance between particles (in units of cell length)
C
Total cell number
Cell-cell adhesion
D
143B
EV
E-cadherin
143B
Aggregates
Single cells
Proportion of cells
EV
E-cadherin
E
U2OS
EV
E-cadherin
U2OS
Aggregates
Single cells
Proportion of cells
EV
E-cadherin